Effects of electrolyte pH and composition on the ethanol electro-oxidation reaction

Stanley C.S. Lai, Steven E.F. Kleijn, Fatma T.Z. Öztürk, Vivienne C. van Rees Vellinga, Jesper Koning, Paramaconi Rodriguez, Marc T.M. Koper*

Leiden Institute of Chemistry, Leiden University, PO Box 9502, 2300 RA Leiden, The Netherlands
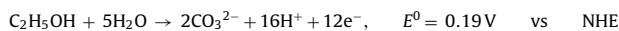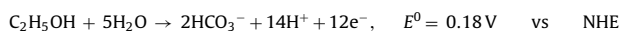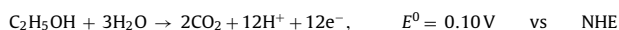
ARTICLE INFO

ABSTRACT

The electrochemical oxidation of ethanol has been studied on platinum and gold electrodes by a combination of electrochemical and spectroscopic techniques in electrolytes of varying pH and composition, the latter primarily determined by the buffering anions. It was found that the activity of reaction increases significantly when the pH of the electrolyte is higher than 10. Furthermore, the results indicate that the selectivity of the reaction depends strongly on the nature of the electrolyte, and, to a smaller extent, on the electrolyte pH. In particular, carbon–carbon bond breaking, which is necessary to achieve full oxidation, could only be observed on platinum in the absence of strongly adsorbing anions. Based on these findings, a tentative general mechanism is suggested and discussed.

© 2010 Elsevier B.V. All rights reserved.

1. Introduction

The increased concerns in the last decades about the future availability of fossil fuels as the main energy source has spurred a renewed interest in the search for alternative energy sources. Low temperature fuel cells are generally considered one of the most promising technologies, since they are able to convert the heat of combustion of a fuel directly into electricity [1]. Traditionally, hydrogen and hydrogen-rich gases are used as a fuel. However, practical difficulties in the production, storage and transportation of hydrogen have barred the widespread adoption of the hydrogen fuel cell. As an alternative to hydrogen, the electrochemical oxidation of small organic molecules containing one or two carbon atoms has been investigated widely [2–11]. In particular, ethanol has received considerable interest due to its low toxicity and the fact that it can be produced in large quantities through the fermentation of biomass. Furthermore, ethanol has a high theoretical energy density of $8.0\,kWh\,kg^{-1}$ [12]. This energy corresponds to the full oxidation of ethanol to carbon dioxide (or (bi)carbonate, depending on the electrolyte pH) at the anode of the fuel cell coupled to the reduction of molecular oxygen at the fuel cell cathode [12]:

$$C_2H_5OH + 3H_2O \rightarrow 2CO_2 + 12H^+ + 12e^-, \qquad E^0 = 0.10\,V \quad vs \quad NHE$$

$$C_2H_5OH + 5H_2O \rightarrow 2HCO_3^- + 14H^+ + 12e^-, \qquad E^0 = 0.18\,V \quad vs \quad NHE$$

$$C_2H_5OH + 5H_2O \rightarrow 2CO_3^{2-} + 16H^+ + 12e^-, \qquad E^0 = 0.19\,V \quad vs \quad NHE$$

$$O_2 + 4H^+ + 4e^- \rightarrow 2H_2O, \qquad E^0 = 1.23\,V \quad vs \quad NHE$$

Since platinum is generally considered the best monometallic catalyst for the electro-oxidation of small organic molecules, and since stable proton-conducting membrane materials, such as Nafion, have been well developed since the 1960s, research on the ethanol electro-oxidation reaction has traditionally focused on platinum electrodes in an acidic electrolyte [10–16]. However, the electro-oxidation of ethanol on platinum in an acidic electrolyte suffers from three (interrelated) issues. First, it is found that, for concentrations that would be sensible for fuel cell applications, the oxidation of ethanol to CO_2 has a minor contribution to the total currents. Rather, the main pathway in the mechanism is the C_2-pathway, in which ethanol is converted to acetaldehyde and, upon further oxidation, to acetic acid, which only yields 2 and 4 electrons per ethanol molecule, respectively [13,14,17]. In addition,

* Corresponding author.
E-mail address: m.koper@chem.leidenuniv.nl (M.T.M. Koper).

acetaldehyde and acetic acid are also unwanted as final products due to their polluting nature. Second, the C_1-pathway, in which ethanol is converted to CO_2, is a complex multistep process. This pathway involves the single carbon intermediates CO_{ad} [14,18–20] and $CH_{(x)ad}$ [20,21], formed by the carbon–carbon bond breaking in ethanol and/or acetaldehyde, and require a high overpotential to be oxidized, thereby directly limiting the potential cell voltage and thereby the total efficiency. Finally, the overall reaction rate for the electro-oxidation of ethanol on platinum in an acidic electrolyte is considered too low for practical purposes.

To circumvent these issues, the effect of varying the composition [11,22–24] and morphology [25,26] of the catalyst as well as the effect of operational parameters such as ethanol concentration [13,14,17] and temperature [25,27] have been investigated extensively. However, studies on the effect of the electrolyte pH on the ethanol electro-oxidation reaction have been far less forthcoming and are generally limited to low (<2) or very high (>12) pH values [28,29], although there are numerous advantages of employing electrolytes which are not strongly acidic. First of all, according to the Nernst equation, the potential range in which water is stable shifts by −59 mV per pH unit. Although this shift is usually circumvented experimentally by using the pH-relative reversible hydrogen electrode (RHE) as a reference electrode, the shift in the absolute potential (or, equivalently, the shift in the work function of the metal electrode) strongly changes the local structure and the electric field at the electrode–electrolyte interface, subsequently causing a change in adsorption strengths [30]. Therefore, the role of adsorption of ions, either from the supporting electrolyte or as a reaction intermediate, is strongly dependent on electrolyte pH. Furthermore, the range of electrode materials that are stable under strongly acidic conditions is very limited, while in neutral and alkaline media less noble and cheaper metals could be considered [31,32]. Finally, since the intermediates and products of the ethanol electro-oxidation reaction can act as acids or bases, it is conceivable that changing electrolyte pH impacts on the stability of intermediates, and thereby on the reaction mechanism and product distribution [33,34].

Despite the significant role of the electrolyte pH on the ethanol oxidation reaction, very few studies have been performed that systemically investigate the full pH range from pH 1 to 13. In this work, we study the role of electrolyte pH on the oxidation of ethanol on gold and platinum electrodes by electrochemical and *in situ* spectroscopic methods.

2. Experimental

All electrochemical measurements were carried out in conventional single-compartment three-electrode glass cells. The cell and all other glassware were cleaned by boiling in 1:1 mixture of concentrated nitric acid and sulfuric acid followed by repeated boiling with ultra-pure water (Millipore MilliQ A10 gradient, 18.2 MΩ cm, 2–4 ppb total organic content) before each experiment. Working solutions were prepared from ethanol (Merck, "Emprove") and supporting electrolyte. The supporting electrolytes employed were perchloric acid solutions ($HClO_4$, Merck, "Suprapur") for the low pH experiments, phosphate buffers from phosphoric acid (H_3PO_4, Fluka, *pro analysis*), sodium dihydrogenphosphate (NaH_2PO_4, Merck, *pro analysis*), sodium hydrogenphosphate (Na_2HPO_4, Merck, *pro analysis*) and/or sodium phosphate (Na_3PO_4, Merck, *pro analysis*) for the intermediate pH experiments and sodium hydroxide (NaOH, Sigma–Aldrich, 99.998%) solutions for high pH experiments. Electrochemical experiments were conducted at room temperature with a computer-controlled Autolab-PGSTAT 12 potentiostat (Ecochemie) or a computer-controlled IviumStat potentiostat (Ivium Technologies).

Rotating disk electrode (RDE) experiments were performed using a Motomatic motor generator.

Fourier Transform Infrared (FTIR) experiments were carried out under external reflection configuration using a Brucker Vertex 80v spectrometer. The cell for spectroelectrochemical experiments was equipped with a CaF_2 prism beveled at 60°. At each potential, 20 interferograms at $8\,cm^{-1}$ were collected using p-polarized light. The reflectance spectra reported are plotted as $(R − R_0)/(R_0)$, where R and R_0 are the reflectance at the sample and at the reference potential, respectively.

Surface enhanced Raman spectroscopic (SERS) measurements were performed with a HR 800 spectrograph (Jobin Yvon) with a holographic grating of $600\,grating\,mm^{-1}$. The confocal hole of the system was set at $100\,\mu m$. A CCD camera with $1024\,pixels \times 256\,pixels$ was used as detector. The excitation line was provided by a 20 mW HeNe laser at 632.8 nm. The laser beam was focused through an Olympus $50\times$ microscope objective, which was not immersed in the electrolyte, into a $5\,\mu m$ spot on the electrode surface. A notch filter was used to filter the SERS signal before reaching the sample. With this configuration, a resolution of $1.2\,cm^{-1}$ was obtained.

The working electrodes used in this study were polycrystalline platinum and gold beads. Prior to each experiment, these working electrodes were flame-annealed before being transferred to the electrochemical cell. The working electrode in the RDE experiments was a platinum disk of 3.175 mm in diameter embedded in a PEEK shroud, which was mechanically polished with alumina (down to $0.3\,\mu m$), rinsed and treated ultrasonically in ultra-pure water before use. The working electrode in the SERS experiments was a gold disk of 5 mm in diameter embedded in a PTFE shroud, which was mechanically polished with alumina (down to $0.3\,\mu m$), rinsed and treated ultrasonically in ultra-pure water before use. The gold electrode was electrochemically roughened [35] before an ultrathin film of a few monolayers of platinum was galvanostatically deposited [36]. The working electrode in the FTIR experiments was a platinum disk of 10 mm in diameter. A platinum or gold foil was employed as the counter electrode in all experiments, while a mercury–mercury sulfate electrode ($Hg/Hg_2SO_4/K_2SO_4$), a mercury–mercury oxide electrode (Hg/HgO/KOH) or a reversible hydrogen electrode (RHE) was used as the reference electrode, depending on the electrolyte. All potentials reported in this paper have been converted to RHE scale in the same electrolyte.

3. Results and discussion

3.1. Ethanol oxidation on platinum

Fig. 1 shows typical cyclic voltammograms for the oxidation of ethanol on platinum in 0.1 M $HClO_4$ (*ca.* pH 1) and 0.1 M NaOH (*ca.* pH 13). Up to 1 V, both electrolytes show essentially the same characteristics: starting at low potentials, the electrode is blocked by adsorbed species originating from the dissociation of ethanol [15], as witnessed by the suppressed currents in the hydrogen underpotential deposition (H_{UPD}) region (0.05–0.40 V). After these adsorbates are stripped oxidatively starting at 0.4–0.5 V, continuous oxidation takes place on a "clean" electrode surface, until the surface is blocked due to the oxidation of the surface (>0.7 V). However, whereas further oxidation of ethanol in alkaline media is completely blocked by the surface oxides, a second oxidation feature can be seen for the acidic electrolyte. After reversing the sweep direction at 1.5 V, the oxidation currents are minimal until the surface oxides are reduced (<0.7 V), leading to a single peak at 0.75 V (in $HClO_4$) or 0.70 V (in NaOH). At potentials below *ca.* 0.4 V, the electrode surface is blocked by ethanol decomposition products again. Although there are similarities between the voltammograms
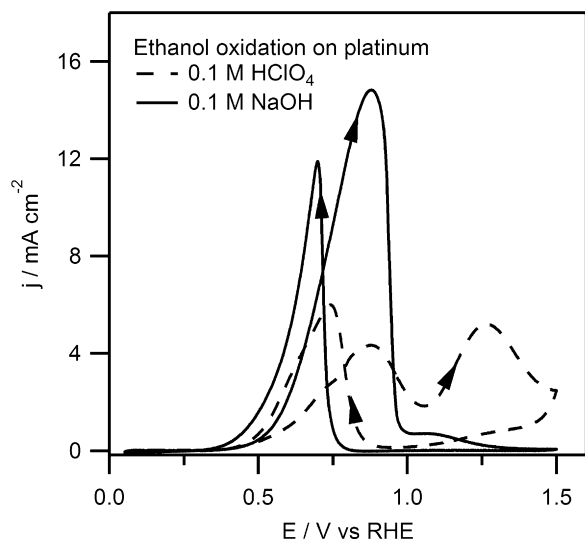
Fig. 1. Cyclic voltammograms (first cycles) for the oxidation of 0.5 M ethanol in 0.1 M HClO$_4$ and 0.1 M NaOH on polycrystalline platinum. The voltammograms are recorded at 50 mV s^{-1}. The arrows indicate the scan direction.

recorded in 0.1 M HClO$_4$ and 0.1 M NaOH, there are also a number of significant differences. First of all, the currents obtained in sodium hydroxide solution are significantly larger than the currents in perchloric media. Furthermore, as mentioned above, the oxidation of ethanol in acidic media shows an oxidation feature in

the oxide region between 1.1 and 1.5 V which is absent in alkaline media. In addition, the voltammogram recorded in sodium hydroxide solution is somewhat shifted to lower potentials compared to the voltammogram recorded in perchloric acid solution. This is most clearly visible in the negative sweep, in which the oxidation feature related to the reduction of the surface oxides is shifted *ca.* 100 mV towards more negative potentials. Similar negative shifts have been observed before and are generally attributed to a higher affinity of OH for the electrode surface in alkaline media [37], leading to a lower onset of surface oxides formation. However, the use of a pH independent reference electrode such as the reversible hydrogen electrode should correct for such 'trivial' pH-effects. Finally, a closer inspection of first oxidation features in the positive scan (between *ca.* 0.4 and 1.0 V) shows that this feature in sodium hydroxide solution consist of a single peak, whereas in perchloric acid solution a small shoulder at 0.70 V can be distinguished.

In order to gain further insight into the effect of the electrolyte pH on the early stages of ethanol oxidation, *in situ* Fourier Transform Infrared (FTIR) spectra were collected during a potential sweep. Since these spectra are recorded relative to a reference spectrum, positive bands (pointing down) correspond to species formed or whose concentration has increased at the sampling potential with respect to the reference potential, while negative bands (pointing up) correspond to the diminution of the concentration. Bipolar bands were found for adsorbed species which are present at the reference and sampling potential and whose frequency is dependent on the potential (Stark effect). Typical spectra recorded during a voltammetric sweep of 10 mV s^{-1} are shown in
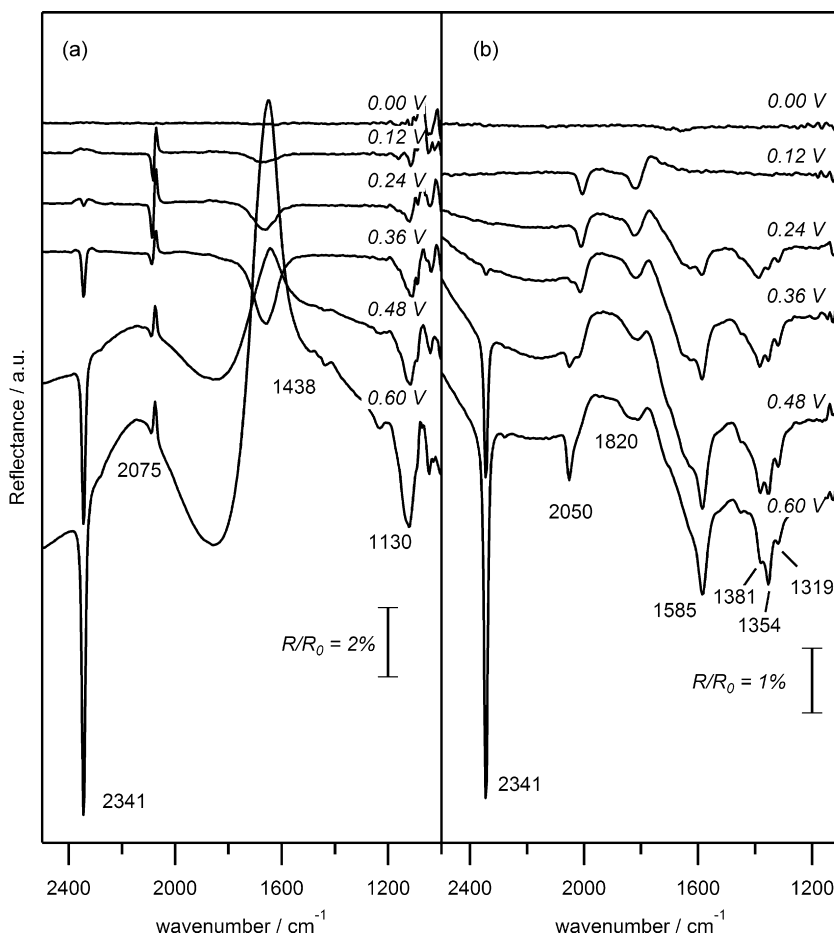

Fig. 2. *In situ* FTIR spectra for the electro-oxidation of ethanol on platinum in (a) 0.1 M HClO$_4$ and (b) 0.1 M NaOH. The reference spectrum was taken at 0.0 V. The sample spectra are measured during a voltammetric sweep at 10 mV s^{-1} at the indicated potentials.

Table 1
Assignment of the FTIR frequencies in the spectra for ethanol oxidation.

Wave number (cm^{-1})	Functional group	Mode
2341	CO_2	O–C–O asymmetric stretching [16,40]
2050–2075	$CO_{l,ad}$	C=O stretching [16,68]
1800–1840	$CO_{b,ad}$	C=O stretching [16,68]
1709	CHO or COOH	C=O stretching of acetaldehyde or acetic acid [16]
~1640	H_2O	H–O–H bending [40]
1585	COO_{ad}	O–C–O asymmetric stretching [41]
1550	COO^-	O–C–O asymmetric stretching [41]
1438	CH_3	CH_3 bending in acetic acid [41]
1415	COO^-	O–C–O symmetric stretching [41]
1381	CH_3	CH_3 bending in acetate [16,41]
1354	CH_3	CH_3 bending in acetaldehyde [16]
1319	HCO_3^-	O–C–O symmetric stretch [44]
1280	COOH	Coupling C–O stretching with O–H deformation [16]
1130	ClO_4^-	O–Cl–O asymmetric stretch [43]

Fig. 2. The reference spectra were recorded at 0.0 V. The frequencies and assignments of the bands are listed in Table 1. From the dipolar band around 2030–2080 cm^{-1}, it can be seen that linearly bonded CO already exists at the reference potential in perchloric acid. This indicates that carbon–carbon bond breaking can occur at low potentials. As can be seen in Fig. 3, the intensity of this band first increases up to 0.20 V. At potentials above 0.20 V, adsorbed CO is slowly oxidized, until *ca.* 0.60 V. At this potential, the CO_L band is completely pointing up, signifying that all CO adsorbed on the surface is oxidized and no more new CO is being formed. This indicates that at higher potentials the CO_{ad} oxidation rate is higher than the C–C bond breaking rate, so that any CO_{ad} that is formed is immediately oxidized. This potential (*ca.* 0.60 V) is in agreement with previously reported studies for the oxidation of ethanol on platinum in perchloric acid [38,39]. Beside the CO band, a band located at 2341 cm^{-1} starts appearing at 0.24 V. The band at 2341 cm^{-1} is typical for the asymmetric O–C–O stretch of carbon dioxides, the oxidation product of CO_{ad} [16,40]. This assignment is further substantiated by the potential dependence of the band intensity (Fig. 3): the appearance and increase of the CO_2 band shows a good correspondence with the decrease of the intensity of the CO_L band. In addition, a band located at 1438 cm^{-1} starts appearing at 0.48 V, although its intensity remains rather low. Based on the fre-

quency, this band can be attributed to CH_3 bending mode of acetic acid [41] or the O–C–O stretching mode of (bidentate) adsorbed acetate [16,41]. Since the position of the band does not depend on the applied potential, which is indicative for a species in solution rather than an adsorbed species, the first assignment seems to be the more likely one. In any case, the appearance of this band can be related to the formation of acetic acid and thus as an indicator for the C_2-pathway of the oxidation mechanism. Furthermore, it should be mentioned that no acetaldehyde bands are observed, although acetaldehyde is an intermediate for acetic acid formation and a potential intermediate for CO_2 formation. The absence of observable features for acetaldehyde could be related to the thin layer configuration of the experimental FTIR set-up, in which the electrode is pressed against the prism to minimize electrolyte interference. In this set-up, this results in a thin layer of electrolyte between the electrode and prism of a few micrometers, causing an inhibition of mass transport between the thin layer and the bulk electrolyte. As a result, intermediate species such as acetaldehyde are trapped in the thin layer, favoring further re-adsorption on the electrode and further reaction towards stable final products like acetic acid and CO_2 [42]. Finally, there is broadband at 1630 cm^{-1} corresponding to the bending mode of water [40] and a sharp band at 1130 cm^{-1} corresponding to the O–Cl–O asymmetric stretching mode of the perchlorate anion [43].

Fig. 2b shows the FTIR spectra recorded during a voltammetric sweep in 0.1 M NaOH. At low potentials, there is a band at *ca.* 2050 cm^{-1} and a bipolar band at *ca.* 1820 cm^{-1}, corresponding to the C–O stretch of linearly adsorbed CO and bridge-bonded CO, respectively. Contrary to perchloric acid media, these bands are still present at 0.60 V, indicating that in alkaline media carbon–carbon bond breaking is faster than CO oxidation at this potential. The bands for the oxidation products of CO_{ad} can be found at 2341 cm^{-1} (CO_2) [40] and 1319 cm^{-1} (adsorbed HCO_3^-) [44]. From the band at 1319 cm^{-1}, it can be seen that the onset of CO_{ad} oxidation is similar to the onset in acidic media. As the reaction proceeds, the local pH drops due to the diffusion limitations in the thin layer, causing CO_2 to be one of the stable products at higher potentials. The formation of adsorbed HCO_3^- also readily explains the presence of CO_{ad} at 0.60 V in alkaline media, even though the onset of oxidation is very similar to acidic media: as CO_{ad} is oxidized at low potentials at the most active sites (*i.e.* the sites that oxidize CO_{ad} at the lowest overpotential) to HCO_3^- (or possibly CO_3^{2-}), the product adsorbs to that surface site. Consequently, this site is effectively blocked for further reaction, forcing further CO_{ad} oxidation to take place at less active sites [45]. Apart from these features, bands for acetaldehyde and acetate can be observed at 1585 cm^{-1} (O–C–O asymmetric stretch of adsorbed acetate [41]), 1381 cm^{-1} (CH_3 bend of acetate [16]) and 1354 cm^{-1} (CH_3 bend of acetaldehyde [16]). Similar to the carbonate band at 1319 cm^{-1}, these bands start appearing at 0.20 V. A
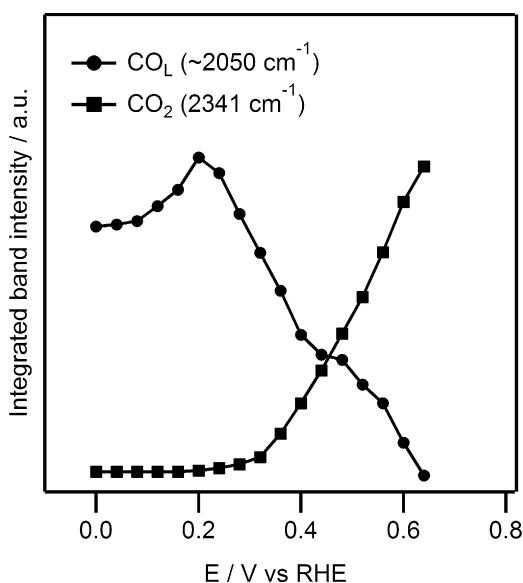

Fig. 3. Integrated band intensities for the bands at ~2050 cm^{-1} (CO_L) and 2341 cm^{-1} (CO_2) measured in FTIR experiments for the oxidation of ethanol in 0.1 M $HClO_4$ on platinum.
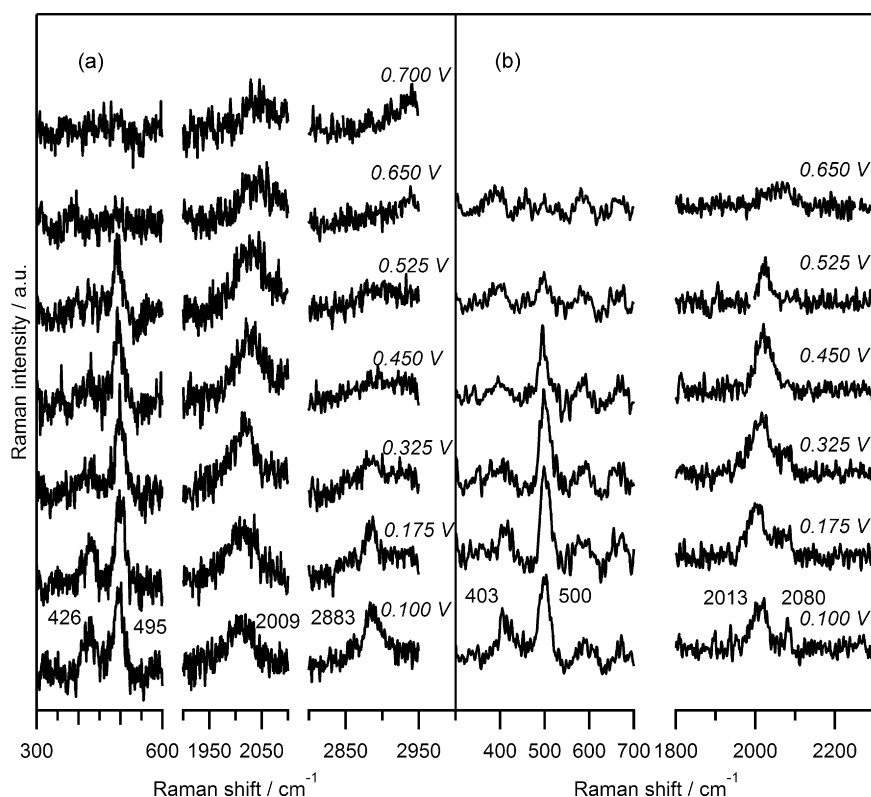
Fig. 4. Surface enhanced Raman spectra of (a) ethanol and (b) deuterated ethanol (ethanol-d_6) dissociation products on a Pt-film electrode in 0.1 M HClO$_4$ recorded at the indicated potentials. Reproduced with permission from Ref. [21].

possible explanation for this behavior is that upon CO$_{ad}$ oxidation the site is blocked by the reaction product (bi)carbonate, blocking it for further CO$_{ad}$ oxidation. However, conversion of ethanol to acetaldehyde and acetic acid might still occur on these sites, since it can be expected that the oxidation of CO$_{ad}$, which requires the formation of a carbon–oxygen bond, might have more stringent conditions for the active site than the conversion of ethanol to acetaldehyde (and possibly the conversion of hydrated acetaldehyde (a geminal C$_2$-diol) [46] to acetic acid), which are 'simple' (i.e. less 'site-demanding') dehydrogenation reactions.

In addition to FTIR spectroscopy, surface enhanced Raman spectroscopy (SERS) was employed to obtain more information on the strongly adsorbed intermediates in the ethanol oxidation reaction on platinum. The results have been described in more details in Ref. [21] (for perchloric acid electrolyte) and Ref. [33] (for sodium hydroxide electrolyte). This section will mostly deal with the main conclusions described there. Before discussing the results, it is important to note that the different approach employed in the SERS experiments compared to the electrochemical and the FTIR experiments. In the SERS experiments, the working electrode consisted of an electrochemically roughened gold electrode covered with a thin platinum film, rather than a bulk platinum electrode. The layer of platinum was thick enough to mask the underlying gold substrate so the (electro)chemical behavior of the platinum electrode can be compared to that of a bulk platinum electrode [36]. Furthermore, to isolate the strongly adsorbed species, ethanol was adsorbed in a separate cell on the electrode at 0.10 V for 15 min before the electrode was transferred to a spectroelectrochemical cell containing only supporting electrolyte (0.1 M HClO$_4$ or 0.1 M NaOH). Instead of sweeping the potential, the potential was increased stepwise between subsequent recordings of SERS spectra.

The results of SERS experiments in 0.1 M HClO$_4$ are displayed in Fig. 4. There are three wave number regions of interest, namely the low-frequency region with two bands at ca. 425 and 500 cm^{-1},

a region with a broad peak around 2000 cm^{-1} and a region with a small peak at low potentials centered on 2880 cm^{-1}. Analogous to the FTIR spectra, the broad peak at 2000 cm^{-1} can be assigned to the C–O stretch of linearly adsorbed CO. Compared to the FTIR spectra, the frequency is slightly lower, indicating a lower CO coverage in the SERS experiments. The peak at ca. 500 cm^{-1} shows the same potential dependence as C–O stretch peak: at potentials below 0.45 V, its intensity increases with potential, while it decreases above 0.45 V. Furthermore, the Pt–C stretch of linearly adsorbed CO at full coverage is generally found around 480 cm^{-1} [47,48]. Therefore, the band at ca. 500 cm^{-1} can be assigned to the Pt–C stretch of linearly adsorbed CO. The small shift to higher wavenumbers is caused by a coverage lower than a complete adlayer, analogous to the shift in the C–O stretching frequency. Similar shifts were also found earlier during the dehydrogenation oxidation of methanol [47] and formic acid to CO [49] and can be readily explained by the fact that the dehydrogenation (and, in the case of ethanol, carbon–carbon bond breaking) of small organic molecules may require a certain ensemble of surface sites [50]. Apart from the CO$_{ad}$ bands, there is another set of band at 425 and 2880 cm^{-1}. These bands show the highest intensity directly after adsorption at low potential (0.10 V) and their intensity decreases monotonously with increasing potential until they disappear completely at 0.45 V, corresponding with the maximum intensity of the CO$_{ad}$ bands. Since frequencies between 2700 and 3000 cm^{-1} are typical for C–H stretching modes [40] and frequencies between 300 and 600 cm^{-1} are typical for metal–adatom stretching modes, the bands at 425 and 2880 cm^{-1} are assigned to the Pt–C stretch and C–H stretch of an adsorbed CH$_x$ species. This assignment is further substantiated by repeating the experiment with ethanol substituted by deuterated ethanol (Fig. 4b). From these experiments, it can be seen that the CO bands are not influenced by deuteration, as would be expected, since CO is a non-hydrogen-containing fragment. The bands at 2880 and 425 cm^{-1}, however, shift to 2080
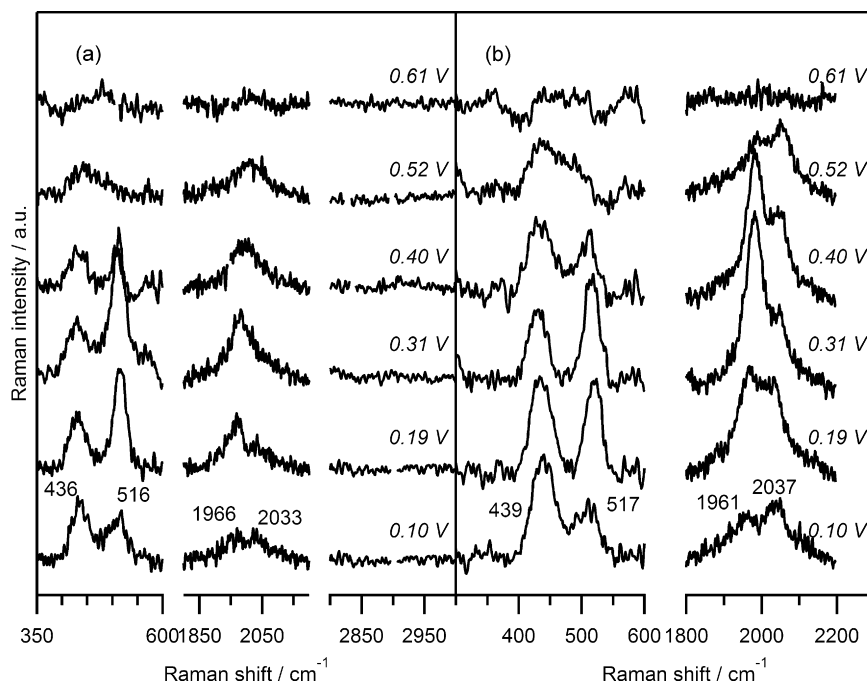
Fig. 5. Surface enhanced Raman spectra of (a) ethanol and (b) deuterated ethanol (ethanol-d_6) dissociation products on a Pt-film electrode in 0.1 M NaOH recorded at the indicated potentials. Reproduced with permission from Ref. [33].
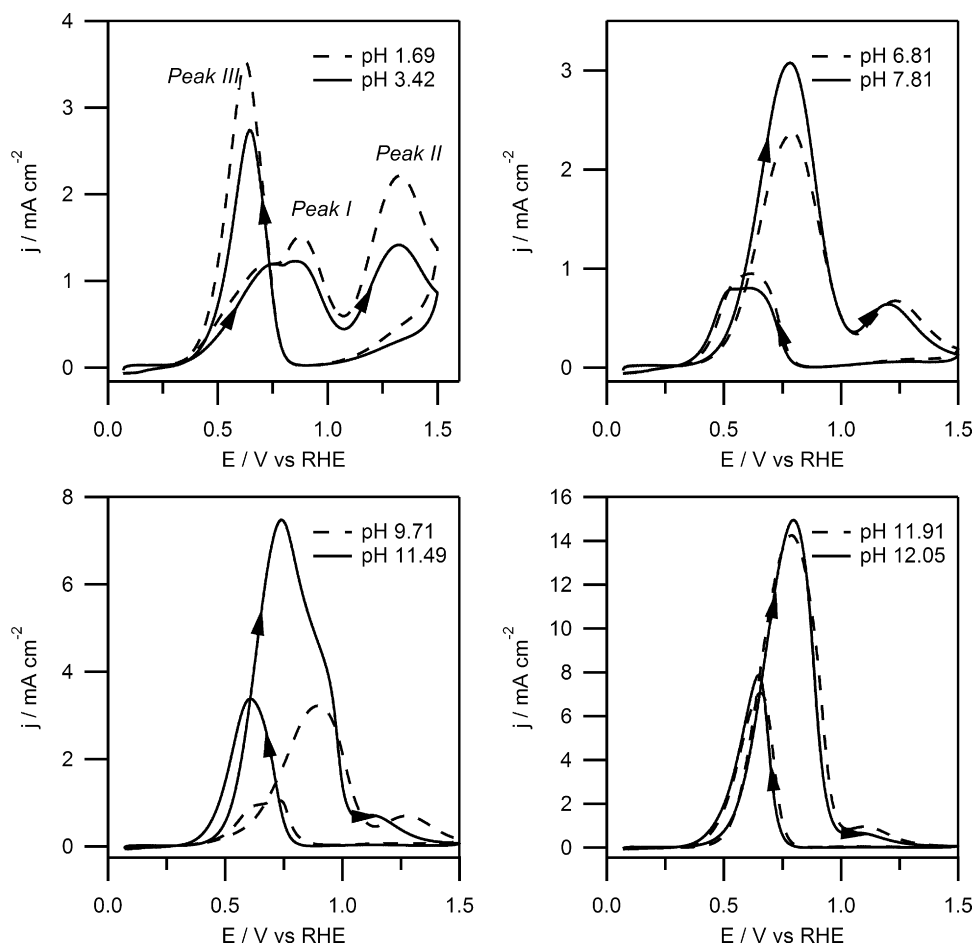

Fig. 6. Cyclic voltammograms for the oxidation of 0.5 M ethanol in 0.1 M phosphate buffers (pH 1–12) on polycrystalline platinum. The voltammograms are recorded at 50 mV s^{-1}. The arrows indicate the scan directions.

and 400 cm^{-1}. Therefore, the band at 2080 cm^{-1} can be assigned to a C–D stretching mode [51] and the band at 400 cm^{-1} can be attributed to the Pt–C stretch of an adsorbed CD$_x$ fragment. Based on the shift, a value of $x = 1$ can be derived [21], which is in agreement with computational [52,53] and ultra-high vacuum studies [54]. Based on these observations, a mechanism for the C$_1$-pathway of ethanol electro-oxidation in acidic media was proposed [21]. In this mechanism, carbon–carbon bond breaking in the ethanol molecule already occurs at low potentials, yielding CH$_{ad}$ and CO$_{ad}$. The adsorbed CH fragment is slowly converted into CO$_{ad}$ between 0.10 and 0.45 V before all CO$_{ad}$ is oxidized between 0.45 and 0.70 V. In addition, it was also established that C–C bond breaking was easier in acetaldehyde than in ethanol.

The same SERS experiments were also conducted in 0.1 M NaOH. Typical spectra are shown in Fig. 5. Again, there are four bands of interest, two bands between 400 and 550 cm^{-1} and two bands around 2000 cm^{-1}. A closer inspection of the bands show that the potential dependency of the intensity of the band at 436 cm^{-1} follows that of the band at 2030 cm^{-1}, and that the intensity of the band at 516 cm^{-1} follows that of the band at 1960 cm^{-1}. In addition, although the relative intensities of the two sets of bands vary with potential, all bands disappear between 0.50 and 0.60 V. Unlike in acidic media, none of these bands shift upon substituting ethanol with deuterated ethanol, indicating that ethanol adsorption does not yield any hydrogen-containing fragments in alkaline media on polycrystalline platinum. Rather, the bands are assigned to two types of CO$_{ad}$. Since there is adsorbed CO, C–C bond breaking does take place in alkaline media. However, rather than yielding CH$_{(x)ad}$ and CO$_{ad}$, only adsorbed CO is observed, indicating that CH$_x$ is unstable on polycrystalline platinum in alkaline media. Surprisingly, on single-crystal electrodes CH$_x$ can be found on surfaces with a low concentration of low-coordination sites [33], suggesting that surface structure is an important factor in the stability of adsorbed CH$_x$ in alkaline media, and that CH$_x$ is converted to CO$_{ad}$ in alkaline media at low-coordination (defect) sites.

The oxidation of ethanol was also studied in 0.1 M phosphate buffers of varying pH, in order to gain more insight on the effect of electrolyte pH. Fig. 6 shows the voltammograms obtained at various pH values. Similar to the voltammetric profile for ethanol oxidation in 0.1 M HClO$_4$ (Fig. 1), the voltammetric profile recorded at pH 2 shows three distinguishable oxidation features. In the positive-going sweep, there is a peak between 0.7 and 1.0 V (hereafter denoted "Peak I") and a peak between 1.1 and 1.5 V (denoted "Peak II"). At pH 2, these two peaks have roughly the same current density. In the negative going sweep, there is a single oxidation peak between 0.7 and 0.4 V ("Peak III"). Comparing the voltammograms recorded the different pH values, it can be seen that the electrolyte pH has a strong influence on the voltammetric profile. This is further illustrated in Fig. 7, in which the peak current densities and peak position of the different peaks are displayed as function of electrolyte pH. It can be seen clearly that all three peaks show markedly different pH dependences. The peak current density of peak I is more or less pH independent below pH 6. From pH 6 to 10, there is a small increase in peak currents which levels at pH 9–10. For pH > 10, there is a strong increase in peak current with increasing pH. Peak II, which we mainly attribute to the further oxidation of acetaldehyde, shows a small decrease with increasing pH below pH 8. For solutions with a pH above 8, the peak current is small and pH independent. Peak III, which has the highest peak current at low pH, has a pH dependence which is similar to that of peak I: at low pH, the peak current is more or less constant up to pH 5–6 while at pH > 10, the peak current increases strongly with increasing pH. At intermediate pH values (pH 5–10), however, peak III is strongly suppressed. Finally, it should be noted that all peaks show a significant shift towards lower potentials at pH > 10, as can be seen by comparing the voltammograms recorded at pH 9.7 and 11.5 (Fig. 6,
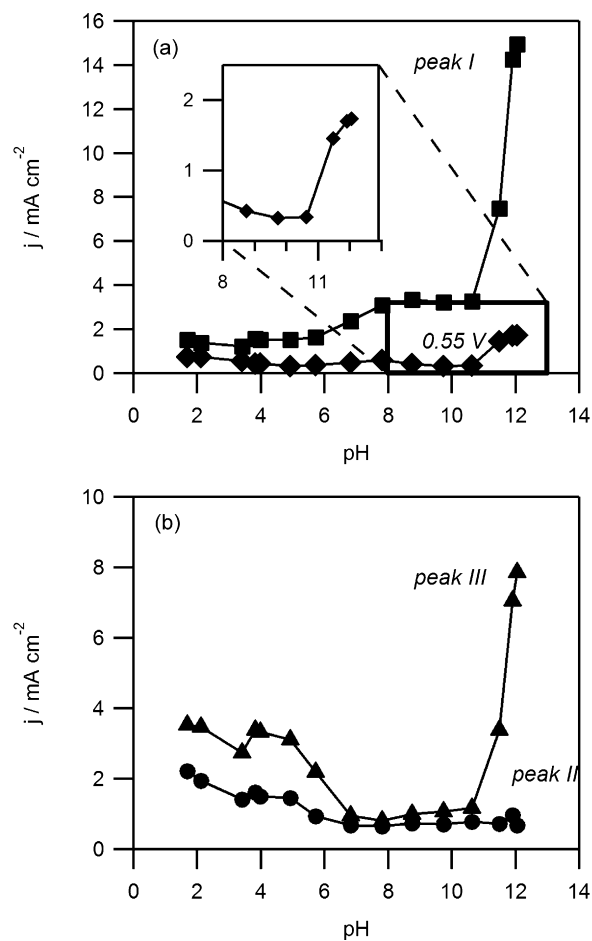

Fig. 7. Peak currents obtained from voltammograms for the oxidation of 0.5 M ethanol in 0.1 M phosphate buffers of pH 2–12. Peaks I and II refer to the first peak (*ca.* 0.9 V) and second peak (*ca.* 1.3 V) in the positive sweep, respectively, while peak III refers to the peak in the negative sweep. In addition, the currents obtained from the voltammograms at a fixed potential of 0.55 V in the positive sweep are also included.

bottom left panel). Similarly, this shift can also been seen when following the current density at a fixed potential of 0.55 V (near the onset of peak I at pH 1), which increases strongly above pH 10, as illustrated in the inset in Fig. 7a.

In addition, rotating disk electrode (RDE) measurements have been performed on the oxidation of ethanol in a 0.1 M phosphate buffer of pH 11.32 in order to study the diffusional properties of the system at alkaline pH. The voltammetric profiles recorded under stationary conditions and at 9 and 16 rotations per second (rps) are shown in Fig. 8. The voltammetric profile with a rotation of 25 rps (not shown) follows those of 9 and 16 rps closely. It can be seen that introducing forced convection to the system results in a small increase in the current densities compared to stationary conditions. However, changing the rotation rate of the electrode has no effect on the current densities, suggesting that the oxidation of ethanol in an alkaline solution is reaction controlled rather than controlled by the mass transport of the reactant species to the electrode, similar to acidic media [16].

Furthermore, although the voltammetric profiles at pH 2 and pH 12 are similar to those in Fig. 1 (pH 1 and 13), as can be expected, it should be noted that the oxidation currents in the phosphate buffer solutions are generally lower than the currents in the perchloric acid and sodium hydroxide solutions. Similar anion effects have been observed earlier to a smaller extent upon changing a perchloric acid solution with a sulfuric acid solution [15] and has
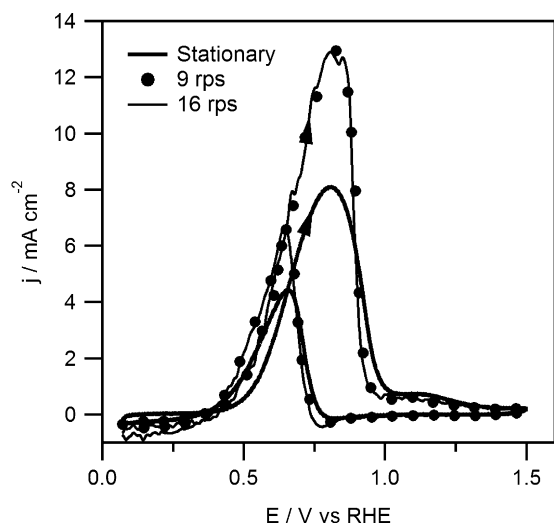
Fig. 8. Cyclic voltammograms for the oxidation of 0.5 M ethanol in 0.1 M phosphate buffers of pH 11.32 recorded under stationary conditions and at rotation rates of 9 and 16 rotations per second. The voltammograms are recorded at 50 mV s^{-1}. The arrows indicate the scan directions.

been related to the difference in adsorption strength of the different anions: whereas perchlorate does not (specifically) adsorb on a platinum surface, sulfate is known to adsorb strongly [55]. Since phosphate adsorbs even more strongly than sulfate [56], it

is not surprising that a significant anion effect on the currents can be observed. Although there is no significant change in the general shape of the voltammetric profile, it is known that anion adsorption can influence the product distribution in electrocatalytic reactions [57]. Therefore, FTIR spectra were also recorded for the early stages of ethanol oxidation in phosphate buffers of pH 2 and pH 12. These FTIR spectra are displayed in Fig. 9. At pH 2, bands corresponding to CO_{ad} (2040 and 1807 cm^{-1}) can be found at potentials higher than 0.40 V. The intensities of this band increases up to 0.785 V, the highest potential measured in this experiment, suggesting that (ethanolic) CO_{ad} is hardly oxidized in a phosphate buffer at potentials below 0.70 V. This is also supported by the absence of a band at 2341 cm^{-1}. Apart from the CO_{ad} bands, bands corresponding to the formation of acetic acid (and possibly acetaldehyde) start developing at 0.70 V at 1709 cm^{-1} (corresponding to a carbonyl stretch [16]) and 1280 cm^{-1} (corresponding to the coupled CO stretching and OH deformation of the carboxylic acid group [16]). At pH 12, no CO_{ad} or CO_2 band can be seen at any potential. Rather, a pair of bands at 1550 and 1415 cm^{-1} start developing at 0.60 V. Since the frequency of these bands does not vary with the applied potential, and the ratio between the two bands is constant, it is likely that both bands belong to the same species in solution. Therefore, we assign the bands at 1550 and 1415 cm^{-1} to the asymmetric and symmetric O–C–O stretch of acetate, respectively.

Comparing the FTIR spectra in Fig. 9, recorded in phosphate buffers of pH 2 and 12, with the FTIR spectra in Fig. 2, recorded in 0.1 M HClO$_4$ and 0.1 M NaOH, it can be seen that the formation and oxidation of CO_{ad} is strongly inhibited in the phosphate
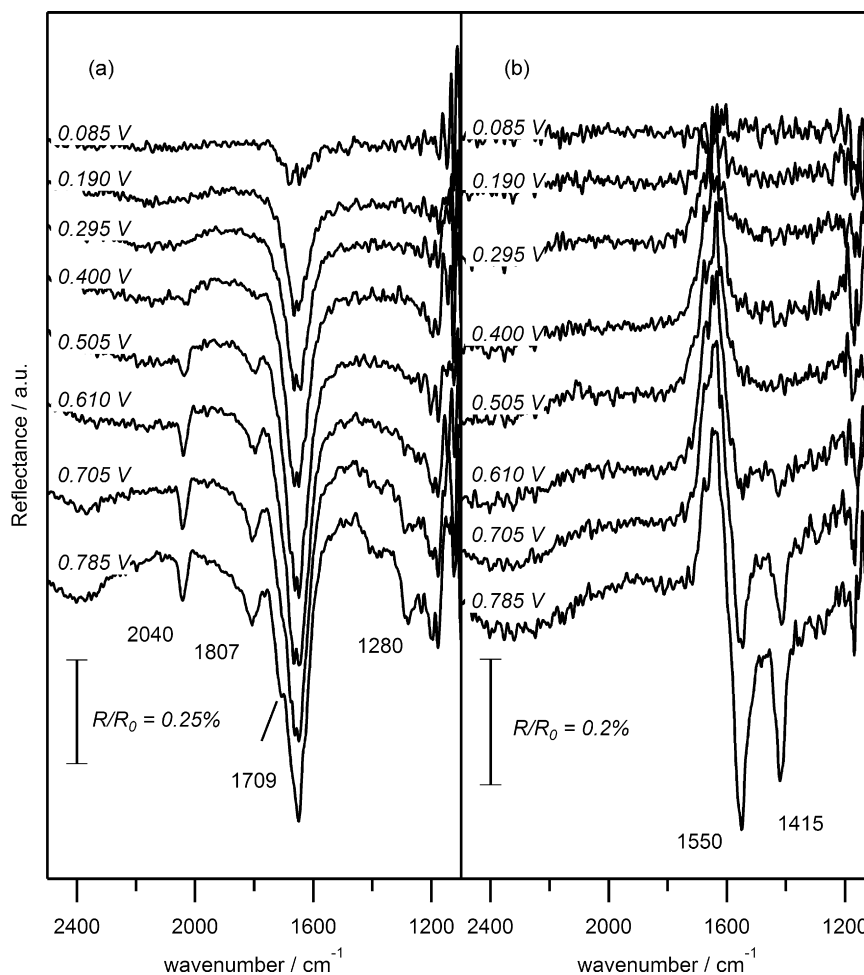

Fig. 9. *In situ* FTIR spectra for the electro-oxidation of ethanol on platinum in a 0.1 M phosphate buffer of (a) pH 2 and (b) pH 12. The reference spectrum was taken at 0.0 V. The sample spectra are measured during a voltammetric sweep at 10 mV s^{-1} at the indicated potentials.
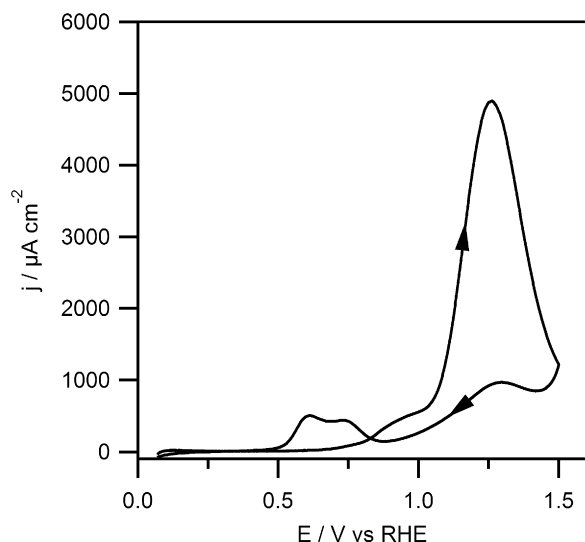
Fig. 10. Cyclic voltammogram for the oxidation of 0.5 M acetaldehyde in 0.1 M $HClO_4$ on polycrystalline platinum. The voltammogram is recorded at 50 mV s^{-1}. The arrows indicate the scan directions.

solutions both at low and at high pH. This result is comparable with studies on methanol oxidation which found that increasing the anion adsorption strength from perchlorate to sulfate decreases the formation of CO_{ad} and increases the formation of soluble partial oxidation products (formaldehyde and formic acid in the case of ethanol) [57–59]. In the case of methanol, it was suggested that an ensemble of (empty) surface sites is required for C–H bond scission, leading to CO_{ad} formation. If such an "ensemble site" was absent, methanol would interact with the surface through O–H bond breaking forming formaldehyde and formic acid. Therefore, increasing the anion adsorption strength would decrease the number of ensemble sites leading to a higher formation rate of the formaldehyde and formic acid. Since it is likely that adsorption, dehydrogenation and subsequent carbon–carbon bond breaking of the ethanol molecule to form CO_{ad} would likewise require a certain ensemble of empty surface sites, and considering that phosphate adsorbs even more strongly than sulfate, it is very probable that CO_{ad} (and thus CO_2) formation is strongly inhibited in a phosphate buffer. Rather, ethanol oxidation in a phosphate media would lead to the formation of acetaldehyde and acetic acid.

Since acetaldehyde (ethanal) is not only a reaction product of the ethanol electro-oxidation reaction, but also an intermediate to further oxidation to either acetic acid or carbon dioxide, it is clear that investigating the oxidation of acetaldehyde may assist in understanding the ethanol electro-oxidation mechanism. It should however be kept in mind that a thorough analysis of the electro-oxidation of acetaldehyde is complicated by the reactivity of acetaldehyde: in an aqueous solution acetaldehyde can be hydrated to a geminal diol ($CH_3CH(OH)_2$) [46]. In equilibrium, about half of the acetaldehyde exists in its hydrated form. Currently, it is unclear whether the active species in the oxidation of acetaldehyde to acetic acid is the hydrated or non-hydrated form of acetaldehyde. In addition, acetaldehyde reacts rapidly in aqueous alkaline media at room temperature for the concentrations used in this study through a base-catalyzed aldol-condensation reaction [60], complicating the matter even further in alkaline electrolytes.

A typical voltammetric profile for the oxidation of acetaldehyde in 0.1 M $HClO_4$ is shown in Fig. 10. Two features can be distinguished in the anodic sweep: at 0.8 V, there is a small shoulder, followed by the main oxidation peak of acetaldehyde between 1.0 and 1.5 V. The negative going sweep shows a small reactivation peak around 0.6 V. Comparing the voltammetric profile of
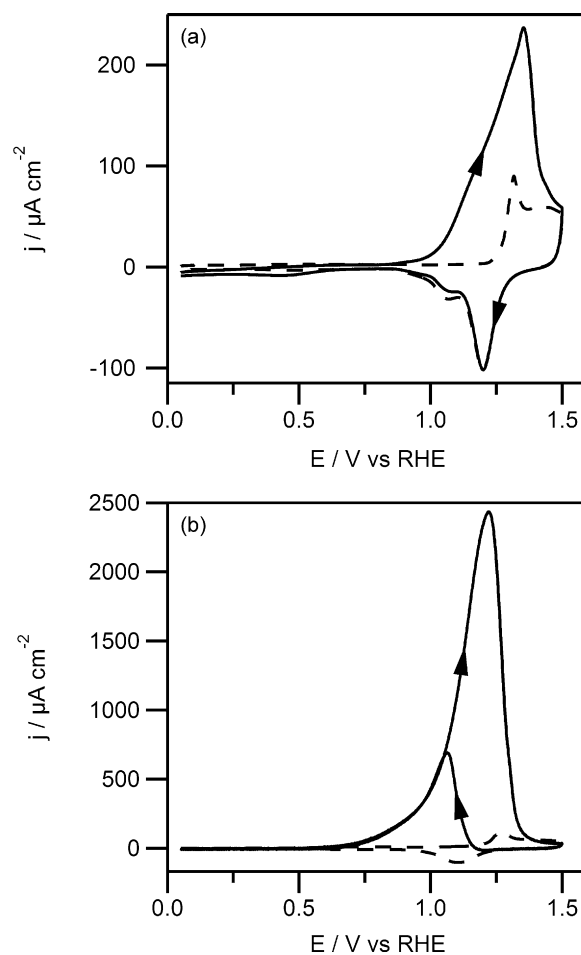

Fig. 11. Cyclic voltammograms for polycrystalline gold in (a) 0.1 M $HClO_4$ and (b) 0.1 M NaOH in the absence (dotted lines) and in the presence of 0.5 M ethanol (solid lines). The voltammograms are recorded at 50 mV s^{-1}. The arrows indicate the scan direction.

acetaldehyde oxidation with that of ethanol oxidation (Fig. 1), a coincidence can be seen in the oxidation feature between 1.0 and 1.5 V. Therefore, we assign the second oxidation peak in the oxidation of ethanol in acidic media to the oxidation of acetaldehyde (or an intermediate derived from acetaldehyde) which is produced in the first oxidation feature (ca. 0.8 V). This assignment might also explain why the oxidation feature between 1.0 and 1.5 V is largely absent in the oxidation ethanol in alkaline media: whereas in acidic media the acetaldehyde that is formed below 1.0 V can be oxidized further above 1.0 V, in alkaline media it is mostly removed from the solution through the aldol-condensation reaction, stopping it from further oxidation. However, some acetaldehyde remains in solution, accounting for the weak oxidation feature at high potentials in the voltammetric profile for the oxidation of ethanol. In both acidic and alkaline media, it should be kept in mind that the first oxidation feature in the ethanol oxidation cannot be attributed solely to the formation of acetaldehyde, as CO_2 and acetic acid are also formed at these potentials as can been seen in the FTIR experiments.

At low acetaldehyde concentrations, acetaldehyde is metastable, allowing for voltammetric measurements at alkaline pH values. These experiments have been performed by Sibille et al. on platinum and gold in solutions of pH 9–14 [61]. On both platinum and gold, it was found that the activity of the acetaldehyde oxidation reaction showed an increase at pH 11. At pH 11–14, the activity roughly followed a sigmoidal (S-shaped) pH dependence with a pH$_{1/2}$ (the pH value which corresponds to the inflection point of the sigmoidal curve) of ca. 13.0. Since this value
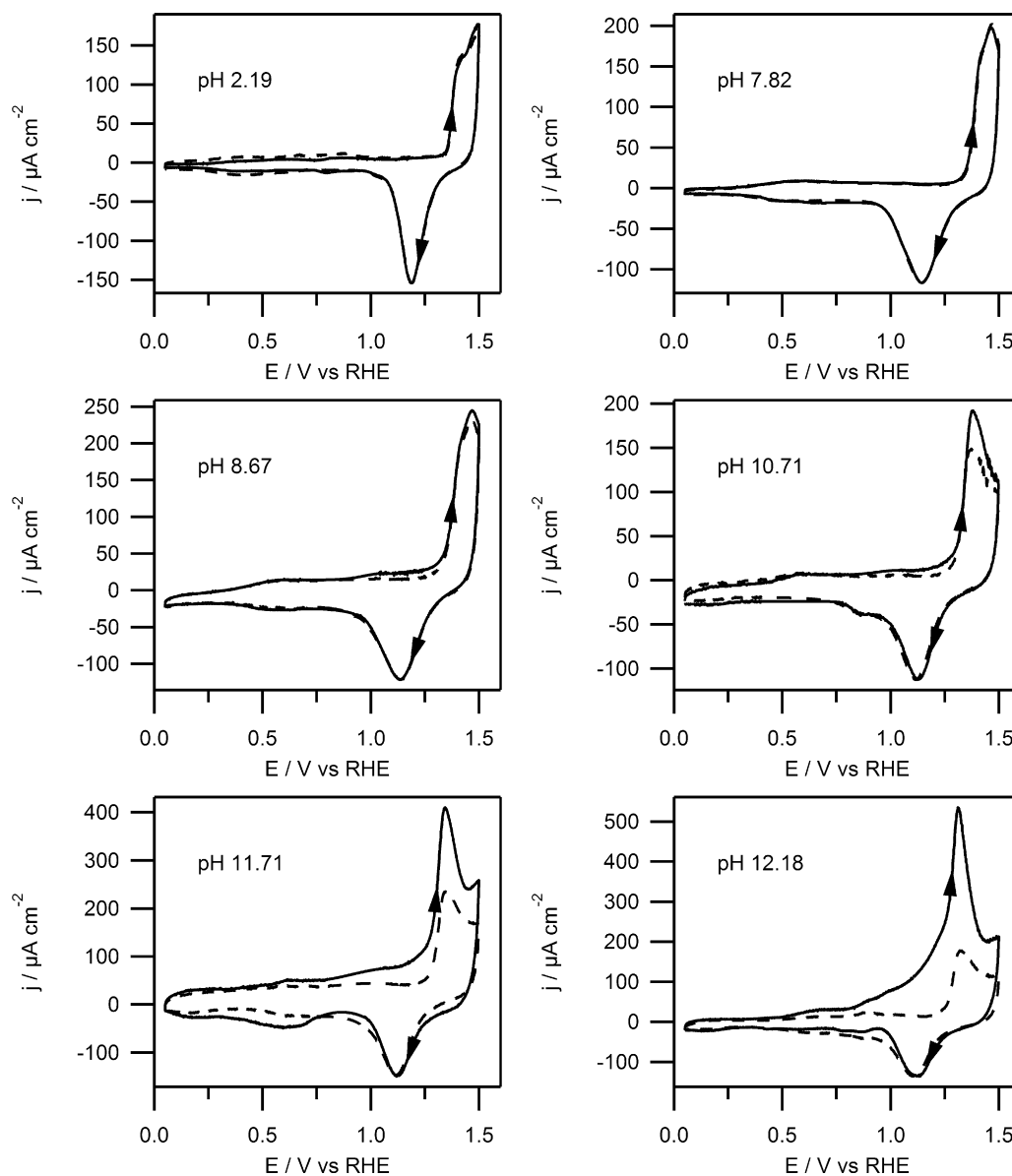
Fig. 12. Cyclic voltammograms for polycrystalline gold in 0.1 M phosphate buffers (pH 2–12) in the absence (dotted lines) and in the presence of 0.5 M ethanol (solid lines). The voltammograms are recorded at 50 mV s^{-1}. The arrows indicate the scan direction.

corresponds nicely to the pK_a of the hydrate of acetaldehyde (13.5), it was concluded that, in alkaline solutions, the active species in the oxidation of acetaldehyde is the geminal anion CH_3CHOHO^-.

3.2. Ethanol oxidation on gold

Gold has been studied much less extensively as an electrocatalyst for the ethanol electro-oxidation. This is mainly due to the fact that gold is a poor catalyst in breaking the carbon–carbon bond, leading to negligible amounts of CO_2, the desired reaction product for the ethanol oxidation reaction [62]. As a model electrocatalyst however, gold allows studying the C_2-pathway of ethanol oxidation (*i.e.* the oxidation of ethanol to acetaldehyde and ultimately to acetic acid/acetate) without interference of the pathways in which the carbon–carbon bond is broken. Typical cyclic voltammograms for the oxidation of ethanol on gold are shown in Fig. 11. A distinct effect of electrolyte pH can be observed by comparing the voltammogram obtained in a 0.1 M perchloric acid solution (*ca.* pH 1) with that obtained in a 0.1 M sodium hydroxide solution (*ca.* pH 13). In perchloric acid, ethanol oxidation starts at *ca.* 0.9 V, before the onset

of surface oxidation as can been in the blank voltammogram. The maximum current occurs at 1.35 V, coinciding with the oxidation of the gold surface, before dropping to the level of the voltammogram recorded in supporting electrolyte only. In the return sweep, no oxidation currents are observed. Rather, the voltammogram recorded with ethanol in solution coincides almost perfectly with the base voltammogram. In a sodium hydroxide solution, the oxidation of ethanol on gold already starts *ca.* 0.6 V, well before the onset of surface oxidation. Upon further increasing the potential, the current rapidly increases until it peaks at 1.25 V. The current density at this potential is about 10 times the value obtained for the oxidation in acidic media. Similar to the oxidation in a perchloric acid solution, the further oxidation of the electrode surface inhibits the oxidation of ethanol. In the return sweep, the currents increase again after the surface oxides are reduced (<1.2 V), unlike the oxidation in acidic media. The currents decay again after reaching a maximum at 1.05 V, coinciding with the currents in the anodic sweep. Since there is no hysteresis between the anodic and cathodic sweep below 1.1 V, it can be deduced that the oxidation of adsorbed species does not play a significant role in the ethanol oxidation reaction on gold
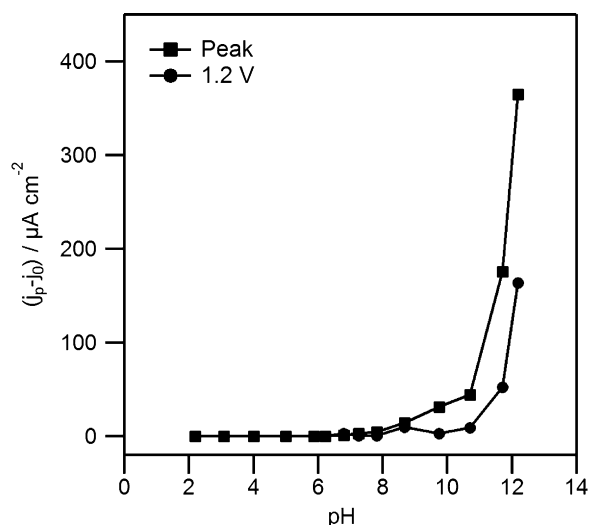
Fig. 13. Corrected peak currents and currents at 1.2 V (see text) obtained from the cyclic voltammograms for the oxidation of 0.5 M ethanol in 0.1 M phosphate buffers of pH 2–12.

in alkaline media [33], which is in agreement with the negligible carbon–carbon bond breaking of ethanol on gold [62].

The effect of electrolyte pH on the ethanol oxidation reaction on gold is further elaborated by employing phosphate buffers. Typical voltammograms at some selected pH values are shown in Fig. 12. It can be seen that the voltammetric response for the electro-oxidation of ethanol on gold in phosphate buffers can be divided into roughly three pH regions. At pH < 6, the voltammograms with ethanol in solution overlap with the blank voltammograms (i.e. voltammograms recorded in the absence of ethanol), demonstrating that ethanol oxidation does not take place at an appreciable rate in this pH range. Starting at pH's higher than 6, the voltammograms start to differ compared to the blank voltammograms. Initially, there is a small increase in the current in the gold surface oxidation region, indicating a small but significant ethanol oxidation rate on the (partially) oxidized surface. The current density in the surface oxidation region increases with pH. This is illustrated more clearly in Fig. 13, which shows the corrected peak current densities (peak current densities from the voltammograms with ethanol

minus the corresponding current density at the same potential in the blank voltammogram) and the corrected current densities at a fixed potential of 1.2 V as a function of pH. It can be seen that at low pH (<6), there is essentially no excess current from the oxidation of ethanol. For pH > 6, the corrected ethanol oxidation (peak) current increases exponentially with pH: an increase of 2.4 pH units increases the corrected peak currents by an order of magnitude. In addition, at higher pH values, an increased current is also visible at lower overpotentials. For example, the onset potential for the oxidation of ethanol on gold is ca. 0.60 V at pH 12.18, the highest pH measured. Furthermore, comparing the voltammograms recorded in phosphate buffers with those recorded in perchloric acid solution and sodium hydroxide solution (Fig. 11) reveals that anion adsorption effects also play a role. Whereas there is no ethanol oxidation activity at low pH values in the phosphate buffer solutions, there already is a significant current due to the oxidation of ethanol in 0.1 M HClO$_4$ (ca. pH 1). Similarly, there is a large difference between the buffer solution of pH 12.18 and the sodium hydroxide solution (ca. pH 13). This is especially notable from the ethanol oxidation current density which is an order of magnitude higher in sodium hydroxide solution than in the phosphate buffer solution. In addition, the voltammogram recorded in sodium hydroxide solution shows a 'reactivation' current in the cathodic scan, which is absent in the phosphate buffer solutions. These effects are very probably related to the high adsorption strength of phosphate [56,63].

4. General discussion and conclusions

In this section, we would like to draw up a detailed mechanistic scheme for the ethanol electro-oxidation reaction based on the results presented here as well as on previously reported data. This mechanism is shown in Scheme 1 and is essentially an extension of our previously proposed mechanism [15]. It incorporates the formation of different reaction products as well as role of electrolyte pH on the stability and reactivity of various intermediates. As mentioned before, two different pathways for the oxidation of ethanol can be distinguished, the C$_2$-pathway and the C$_1$-pathway. We shall discuss each pathway separately before remarking on the overall mechanism.

In the C$_2$-pathway, the carbon–carbon bond of ethanol remains intact upon oxidation. Rather, ethanol is converted to acetaldehyde and eventually to acetic acid/acetate. It is well accepted that this
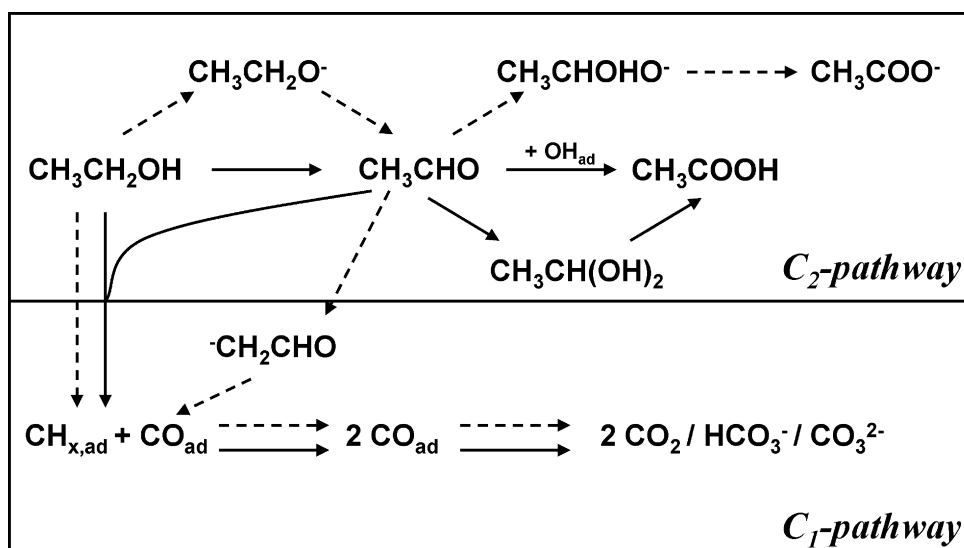
Scheme 1. Proposed reaction mechanism for the ethanol electro-oxidation reaction. Solid arrows denote the mechanism at low electrolyte pH, while dashed arrows denote the mechanism at high electrolyte pH.

is the main pathway for the oxidation of ethanol on gold [62]. In addition, the FTIR experiments discussed in this paper show that the C_2-pathway is also the preferred pathways for the oxidation of ethanol on platinum in the presence of strongly adsorbing anions, such as phosphates, suggesting that this pathway requires a smaller or different 'ensemble site' than the C_1-pathway. It has been suggested that this pathway is initiated by the cleavage of the O–H bond of ethanol at the metal surface leading to adsorbed ethoxy, both in electrochemical [62,64] and ultra-high vacuum [54] studies. The adsorbed ethoxy is subsequently converted to acetaldehyde through a simple dehydrogenation step. Acetaldehyde can then either diffuse into the bulk of the solution or remain near the electrode surface for further oxidation to acetic acid. At the moment, relatively little is known about which 'form' of acetaldehyde is the active species for its conversion to acetic acid, at least in acidic media. On the one hand, it has been suggested that acetaldehyde (as CH_3CHO) reacts directly with a surface oxygenated species to form acetic acid, since the potential region in which the oxidation takes place corresponds to a partially oxidized surface [17,62]. Alternatively, acetaldehyde is readily hydrated in an aqueous solution, forming the geminal diol ($CH_3CH(OH)_2$), which can de dehydrogenated to acetic acid [62]. At present, it has not been possible to unambiguously determine which of these two paths is the dominant one.

There are several effects of electrolyte pH on the C_2-pathway. First of all, as shown by Sibille et al. [61], the conversion of acetaldehyde to acetate showed an increase with pH between 10 and 14. By relating these findings with the pK_a of the gem-diol of acetaldehyde it was concluded that, at high pH, the main reactive species for the oxidation of acetaldehyde is the deprotonated form of the geminal diol (CH_3CHOHO^-). Similarly, we propose that, at high pH, ethoxy (in solution) is the dominant reactant species for oxidation to acetaldehyde rather than ethanol. As can be seen in Figs. 7 and 13, the ethanol oxidation activity increases strongly at *ca.* pH 11. As ethanol has a pK_a of *ca.* 15 [65], a solution pH of 11 would more or less correspond to the lower limit at which there is a non-negligible concentration of ethoxy. Since it is likely that the first step of the oxidation of ethanol to acetaldehyde requires the formation of an adsorbed ethoxy species, this would readily explain the increase in strong increase in activity at pH > 11, as at that pH the formation of acetaldehyde is essentially a single dehydrogenation step, as opposed to lower solution pH where it requires two dehydrogenation steps. It should be kept in mind, however, that an important implication of this mechanism is that the strong increase in current in alkaline media is mainly related to an increased formation of acetaldehyde. In addition, it should be noted that although the equilibrium concentration of ethoxy at pH 11 is in the sub-millimolar range, the reaction does not reach diffusion control, which can be probably be attributed to fast kinetics of the (ethanol-ethoxy) acid–base equilibrium. Finally, the pH of the electrolyte solution also impacts the stability of acetaldehyde, as it can rapidly react through an aldol-condensation reaction in alkaline media, deactivating it for further reaction.

In the C_1-pathway, the carbon–carbon bond can be broken in ethanol or acetaldehyde [21], leading eventually to carbon dioxide (or (bi)carbonate). This pathway is mainly noticeable on platinum electrodes in the absence of a strongly adsorbing anion, such as in perchloric acid solution or sodium hydroxide solution, although the contribution of this pathway to the total current is still small [13]. In this pathway, the carbon–carbon bond is broken at low potentials, resulting in adsorbed single carbon fragments, as can be seen in the SERS and (partially) in the FTIR experiments. Although these adsorbed fragments can be obtained both from ethanol and acetaldehyde, our findings have shown that it is more facile in acetaldehyde, suggesting that C–C bond breaking occurs through an acetaldehyde-like intermediate rather than directly within the

ethanol molecule [21]. Regardless of their molecular precursor, the adsorbed C_1-species are initially $CH_{x,ad}$ (with $x = 1$ in an acidic electrolyte) and CO_{ad}. As the potential is increased, the CH_x fragments are oxidized to CO_{ad} before being oxidized to CO_2 (or (bi)carbonate, depending on the electrolyte pH). Apart from influencing the final product, the electrolyte pH also has other effects on the C_1-pathway of ethanol oxidation. It was found that the reactivity of $CH_{x,ad}$ is strongly dependent on the electrolyte pH: in acidic media, CH_{ad} could be observed as a stable intermediate between *ca.* 0.10 and 0.45 V regardless of surface structure [15,21]. In alkaline media, on the other hand, CH_x could only be observed on single-crystal electrodes with relatively long terraces. On electrodes with a high density of low-coordination sites, such as polycrystalline electrodes, only adsorbed CO was found, implying that on these sites $CH_{x,ad}$ was rapidly converted to CO_{ad} upon adsorption [33]. In addition, it has been reported that the selectivity towards the C_1-pathway may be enhanced in alkaline media [34], indicating that C–C bond breaking is more facile in alkaline media. This finding can likely be explained by considering acid/base properties of acetaldehyde, which is the most likely candidate for C–C bond breaking. In acetaldehyde, the α-hydrogen atom (in the CH_3 group) is slightly acidic with a pK_a of *ca.* 17 [66]. Therefore, in electrolytes with a high pH, acetaldehyde can be deprotonated, yielding a $[CH_2CHO]^-$ anion, in which the negative charge is delocalized. This can also be witnessed by the occurrence of the aldol-condensation reaction, of which the deprotonation of the α-hydrogen atom is the first step. As a result of the deprotonation, the carbon–carbon bond is less shielded and therefore more easily accessible for bond breaking at the electrode surface. This enhanced carbon–carbon bond breaking, combined fact that the $CH_{x,ad}$ [33] and CO_{ad} [67] can be oxidized at lower overpotentials in alkaline media compared to acidic media readily explains why the selectivity towards the C_1-pathway is enhanced in alkaline media. On the other hand, we note that Behm et al. have recently suggested that the main parameter to affect C–C bond breaking in ethanol oxidation is temperature [27], higher temperatures leading to an enhanced CO_2 efficiency (up to 50%). Given that the cited study in alkaline media [34] was conducted at 60 °C, we believe that the question of how to improve C–C bond breaking at room temperature remains largely open.

Acknowledgments

References

[1] Handbook of Fuel Cells: Fundamentals, Technology and Applications, John Wiley and Sons, Chichester, England, 2003.
[2] S. Wasmus, A. Küver, J. Electroanal. Chem. 461 (1999) 14.
[3] A.V. Tripkovic, K.D. Popovic, B.N. Grgur, B. Blizanac, P.N. Ross, N.M. Markovic, Electrochim. Acta 47 (2002) 3707.
[4] A. Capon, R. Parsons, J. Electroanal. Chem. 44 (1973) 239.
[5] C. Rice, R.I. Ha, R.I. Masel, P. Waszczuk, A. Wieckowski, T. Barnard, J. Power Sources 111 (2002) 83.
[6] J.T. Muller, P.M. Urban, W.F. Holderich, K.M. Colbow, J. Zhang, D.P. Wilkinson, J. Electrochem. Soc. 147 (2000) 4058.
[7] M.M. Mench, H.M. Chance, C.Y. Wang, J. Electrochem. Soc. 151 (2004) A144.
[8] J.M. Orts, A. Fernandez-Vega, J.M. Feliu, A. Aldaz, J. Clavilier, J. Electroanal. Chem. 290 (1990) 119.
[9] H. Wang, Z. Jusys, R.J. Behm, J. Electroanal. Chem. 595 (2006) 23.
[10] C. Lamy, A. Lima, V. LeRhun, F. Delime, C. Coutanceau, J.-M. Léger, J. Power Sources 105 (2002) 283.
[11] E. Antolini, J. Power Sources 170 (2007) 1.
[12] F. Vigier, C. Coutanceau, F. Hahn, E.M. Belgsir, C. Lamy, J. Electroanal. Chem. 563 (2004) 81.
[13] G.A. Camara, T. Iwasita, J. Electroanal. Chem. 578 (2005) 315.
[14] S.C. Chang, L.W.H. Leung, M.J. Weaver, J. Phys. Chem. 94 (1990) 6013.
[15] S.C.S. Lai, M.T.M. Koper, Faraday Discuss. 140 (2008) 399.

[16] F. Colmati, G. Tremiliosi-Filho, E.R. Gonzalez, A. Berna, E. Herrero, J.M. Feliu, Faraday Discuss. 140 (2008) 379.
[17] M.J.S. Farias, G.A. Camara, A.A. Tanaka, T. Iwasita, J. Electroanal. Chem. 600 (2007) 236.
[18] X.H. Xia, H.D. Liess, T. Iwasita, J. Electroanal. Chem. 437 (1997) 233.
[19] Q. Wang, G.Q. Sun, L.H. Jiang, Q. Xin, S.G. Sun, Y.X. Jiang, S.P. Chen, Z. Jusys, R.J. Behm, Phys. Chem. Chem. Phys. 9 (2007) 2686.
[20] J. Shin, W.J. Tornquist, C. Korzeniewski, C.S. Hoaglund, Surf. Sci. 364 (1996) 122.
[21] S.C.S. Lai, S.E.F. Kleyn, V. Rosca, M.T.M. Koper, J. Phys. Chem. C 112 (2008) 19080.
[22] W.J. Zhou, W.Z. Li, S.Q. Song, Z.H. Zhou, L.H. Jiang, G.Q. Sun, Q. Xin, K. Poulianitis, S. Kontou, P. Tsiakaras, J. Power Sources 131 (2004) 217.
[23] J.M. Leger, S. Rousseau, C. Coutanceau, F. Hahn, C. Lamy, Electrochim. Acta 50 (2005) 5118.
[24] C. Lamy, S. Rousseau, E.M. Belgsir, C. Coutanceau, J.M. Léger, Electrochim. Acta 49 (2004) 3901.
[25] F.H.B. Lima, D. Profeti, W.H. Lizcano-Valbuena, E.A. Ticianelli, E.R. Gonzalez, J. Electroanal. Chem. 617 (2008) 121.
[26] S.-B. Han, Y.-J. Song, J.-M. Lee, J.-Y. Kim, K.-W. Park, Electrochem. Commun. 10 (2008) 1044.
[27] S. Sun, M.C. Halseid, M. Heinen, Z. Jusys, R.J. Behm, J. Power Sources 190 (2009) 2.
[28] M.C. Morin, C. Lamy, J.M. Léger, J.L. Vasquez, A. Aldaz, J. Electroanal. Chem. 283 (1990) 287.
[29] M. López-Atalaya, E. Morallón, F. Cases, J.L. Vázquez, J.M. Pérez, J. Power Sources 52 (1994) 109.
[30] S.A. Wasileski, M.T.M. Koper, M.J. Weaver, J. Phys. Chem. B 105 (2001) 3518.
[31] Y. Kiros, S. Schwartz, J. Power Sources 87 (2000) 101.
[32] J.W. Kim, S.M. Park, J. Electrochem. Soc. 150 (2003) E560.
[33] S.C.S. Lai, M.T.M. Koper, Phys. Chem. Chem. Phys. 11 (2009) 10446.
[34] V. Rao, Hariyanto, C. Cremers, U. Stimming, Fuel Cells 7 (2007) 417.
[35] P. Gao, D. Gosztola, L.W.H. Leung, M.J. Weaver, J. Electroanal. Chem. 233 (1987) 211.
[36] S. Zou, M.J. Weaver, Anal. Chem. 70 (1998) 2387.
[37] J.S. Spendelow, J.D. Goodpaster, P.J.A. Kenis, A. Wieckowski, J. Phys. Chem. B 110 (2006) 9545.
[38] V. Pacheco Santos, V. Del Colle, R. Batista de Lima, G. Tremiliosi-Filho, Electrochim. Acta 52 (2007) 2376.
[39] J.F. Gomes, B. Busson, A. Tadjeddine, G. Tremiliosi-Filho, Electrochim. Acta 53 (2008) 6899.
[40] G. Socrates, Infrared Characteristic Group Frequencies, Wiley-Interscience, New York, 1980.
[41] F. Quilès, A. Burneau, Vib. Spectrosc. 16 (1998) 105.
[42] Y.E. Seidel, A. Schneider, Z. Jusys, B. Wickman, B. Kasemo, R.J. Behm, Faraday Discuss 140 (2008) 167.
[43] S. Pandiarajan, R.K. Rajaram, V. Ramakrishnan, J. Raman Spectrosc. 36 (2005) 785.
[44] T. Iwasita, A. Rodes, E. Pastor, J. Electroanal. Chem. 383 (1995) 181.
[45] G. García, P. Rodríguez, V. Rosca, M.T.M. Koper, Langmuir (2009), doi:10.1021/la902251z.
[46] R.P. Bell, B.D. Darwent, Trans. Faraday Soc. 46 (1950) 34.
[47] F.J.E. Scheijen, G.L. Beltramo, S. Hoeppener, T.H.M. Housmans, M.T.M. Koper, J. Solid State Electrochem. 12 (2008) 483.
[48] S. Zou, M.J. Weaver, J. Phys. Chem. 100 (1996) 4237.
[49] B. Ren, X.B. Lian, J.F. Li, P.P. Fang, Q.P. Lai, Z.Q. Tian, Faraday Discuss. 140 (2008) 155.
[50] A. Cuesta, J. Am. Chem. Soc. 128 (2006) 13332.
[51] S. Pinchas, I. Laulicht, Infrared Spectra of Labelled Compounds, Academic Press, London, 1971.
[52] R. Alcala, M. Mavrikakis, J.A. Dumesic, J. Catal. 218 (2003) 178.
[53] K.I. Gursahani, R. Alcala, R.D. Cortright, J.A. Dumesic, Appl. Catal. A: Gen. 222 (2001) 369.
[54] A.F. Lee, D.E. Gawthrope, N.J. Hart, K. Wilson, Surf. Sci. 548 (2004) 200.
[55] J. Mostany, E. Herrero, J.M. Feliu, J. Lipkowski, J. Phys. Chem. B 106 (2002) 12787.
[56] J. Mostany, P. Martínez, V. Climent, E. Herrero, J.M. Feliu, Electrochim. Acta 54 (2009) 5836.
[57] T.H.M. Housmans, A.H. Wonders, M.T.M. Koper, J. Phys. Chem. B 110 (2006) 10021.
[58] E.A. Batista, G.R.P. Malpass, A.J. Motheo, T. Iwasita, J. Electroanal. Chem. 571 (2004) 273.
[59] E.A. Batista, G.R.P. Malpass, A.J. Motheo, T. Iwasita, Electrochem. Commun. 5 (2003) 843.
[60] J.P. Guthrie, Can. J. Chem., Rev. Can. Chim. 52 (1974) 2037.
[61] S. Sibille, J. Moiroux, J.-C. Marot, S. Deycard, J. Electroanal. Chem. 88 (1978) 105.
[62] G. Tremiliosi-Filho, E.R. Gonzalez, A.J. Motheo, E.M. Belgsir, J.M. Leger, C. Lamy, J. Electroanal. Chem. 444 (1998) 31.
[63] A. Cuesta, M. Kleinert, D.M. Kolb, Phys. Chem. Chem. Phys. 2 (2000) 5684.
[64] T. Iwasita, E. Pastor, Electrochim. Acta 39 (1994) 531.
[65] P. Ballinger, F.A. Long, J. Am. Chem. Soc. 82 (1960) 795.
[66] J.P. Guthrie, J. Cossar, Can. J. Chem., Rev. Can. Chim. 64 (1986) 2470.
[67] G. García, M.T.M. Koper, Phys. Chem. Chem. Phys. 10 (2008) 3802.
[68] M.H. Shao, R.R. Adzic, Electrochim. Acta 50 (2005) 2415.